©2017

Mustafa Kanaan Alazzawi

ALL RIGHTS RESERVED

EVALUATION OF THE EFFECT OF EXTRUSION VELOCITY AND PASTE WATER CONTENT ON THE MICROSTRUCTURAL VARIABILITY AND GREEN STRENGTH OF EXTRUDED TITANIUM DIOXIDE

by

MUSTAFA KANAAN ALAZZAWI

A thesis submitted to the

Graduate School- New Brunswick

Rutgers, The State University of New Jersey

In partial fulfillment of the requirements

For the degree of

Master of Science

Graduate Program in Materials Science and Engineering

Written under the direction of

Dr. Richard A. Haber

And approved by

_____

_____

_____

New Brunswick, New Jersey

October, 2017

ABSTRACT OF THE THESIS

Evaluation of the Effect of Extrusion Velocity and Paste Water Content on the Microstructural Variability and Green Strength of Extruded Titanium Dioxide

By MUSTAFA KANAAN ALAZZAWI

Thesis Director:

Richard A. Haber

Extrusion processes are used to form porous materials such as a catalyst supports. They are important in purifying the harmful gas emissions. Titanium dioxide is widely used as an extruded support because of its favorable properties such as high catalytic activity, high thermal, and chemical stability. Catalyst supports are used wildly in industries relating to automobiles, petroleum refining, and energy production where a high catalytic performance is essential. The catalytic performance and species diffusivity are affected by the microstructural variability and pore interconnectivity. Extrusion processes pose problems in the spatial variation of porosity and green strength of extrudate. Typically, the size distribution of an extrudate is measured and quantified using either a helium or mercury porosimetry, but both fail to quantify the spatial variation of porosity. Measuring the handling strength of an extrudate fails to provide a high level of precision that can be obtained from measuring the green strength of extrudate. In this thesis, the water content

effect on the green strength and microstructure of extrudate was examined. A quantitative approach using 2-D visualization and segmentation was developed to quantify the spatial variation of porosity. The effect of extrusion velocity on the green strength and spatial variation of porosity of extrudate was also assessed.

A wide range of water content and varying binder content of paste were analyzed using torque and capillary rheometer to determine the effect of water content. The effect was evaluated using SEM and green strength measurements. A range of extrusion velocities (shear rates) were conducted on two different paste formulations. Their effect on the spatial variation of porosity in the sheared region (at the die wall) compared to the unsheared region of the extrudate was quantified using a 2-D visualization and segmentation approach. The green strength measurements were also conducted on extrudates to evaluate the effect of extrusion velocity on the green strength.

The green strength measurements revealed that there is a clear relationship between the water content of paste and green strength of extrudate, where a high water content results in a high green strength. A relationship between the green strength and extrusion velocity of the extrudate was observed where a high extrusion velocity, the green strength of extrudate decreases because of high shear and ineffective particle arrangement.

SEM images showed a reduction in agglomerate size and porosity as a result of high water content. Varying the extrusion velocity has a large effect on the spatial variation of porosity of extrudate. Image analysis showed a low porosity in the sheared region (at the die wall) compared to an unsheared region for samples that were extruded at a low velocity. Conversely, high porosity is observed in the sheared region (at the die wall) compared to an unsheared region for samples that were extruded at a high velocity.

Acknowledgement

A special thank you to Dr. Richard A. Haber. This would not be possible without his gaudiness, support, and mentorship. I have learned and grew up more because of his insights and advises. I would not be where I am today without him believing in me. Thanks, Dr. Haber.

Thank you, Dr. M. John Mathewson and Dr. Dunbar P. Birnie for being on my thesis committee.

A huge thank you to Michelle, who was always being there for me and for everyone. Thanks for the cup of tea and for your support in bad and good times. Our works will not be done and we will not be able to move forward without you. I would like also to thank Laura, I will keep smiling.

I would like to thank Sukanya, who has been helpful through my graduate school. You are a very wonderful friend. She always had provided insights and helped me to reach this point.

At Rutgers University, I had a wonderful opportunity to meet wonderful friends. Ian, Joe, and Vince who are not just my officemate but also my friends. Thanks for a great time at work. They helped me to accomplish this. They have been there for me. I would like also to thank everyone in Dr. Haber research group.

Ian, you are a very dear friend. I am so glad that Dr. Haber did put us together in the same group. You have never ever turned your back on me. You have always been there for me. I am so grateful for our friendship. Thanks, Ian.

I would like to especially thank Eric Bennett, John Casola, and Chuck Rohn for their help and technical assistance. Thanks to Malvern Instruments Ltd. for providing the equipment.

I would like to thank the undergraduate assistants for their help. Thank you, Frank, Priya, Nirali, Ojaswi, and Kaavya.

I would like to thank all professors, teachers, and friends who have/had been in my life here or at home. Who shaped me and become who I am today.

I would like to acknowledge the Ceramic, Composite, and Optical Materials Center (CCOMC). Also, I would like to acknowledge The Higher Committee for Education Development in Iraq (HCED) for the scholarship.

My beloved sisters, Dua'a and Israa, thank you for everything and for the love you have given me. To my family especially my grandma, I miss you.

To my very special people in my life, my dad, Kanaan, and my mom, Wafa. Who have been inspiring me. Your love has given me the courage to overcome any challenges in my life and to reach any accomplishments. This work and who I am today is a reflection of your hard work. I love you. I would like to dedicate this work to you, mom and dad.

Preface

The thesis is partially from the conference paper,

> M. Alazzawi and R. Haber, "The effect of paste water content on the green microstructure of extruded titanium dioxide," *Processing, Properties, and Design of Advanced Ceramics and Composites: Ceramic Transactions,* vol. 261, in press.

A majority of the thesis is pending publication in a scientific journal.

Table of Contents

List of Tables

List of Figures

1. Introduction

Environmental pollution has been a major concern for the past few decades. The air pollution has posed environmental issues since the industrial revolution. On a daily basis there are dozens of harmful gases contribute in climate change and global warming [1, 2]. The harmful emissions can be purified using catalytic converters and membranes [3, 4]. Extrusion processes are used to produce a honeycomb catalytic converters to support an active component [3-5].

Extrusion processes can cause inhomogeneity and microstructural variations in a material. High quality extrusion products depend on die geometry, extrusion velocity, and paste rheology properties [6]. The production processes can cause severe variations in the microstructure which can lead to fractures, uneven pores, and agglomerations especially in a complex system. The agglomerations can impede the active sites of catalysts [7]. The selectivity and activity of the catalysts is highly dependent on porosity and pore size distribution in the catalysts [8]. Additionally, species diffusivity in catalysts materials is influenced by many factors such as pore volume and distribution [8-11].

1.1. Capillary, Torque Rheometer, and Paste Flow

In assessing the extrudability of a paste, common analytical methods include both torque and capillary rheometer. The torque rheometer uses to evaluate the rheological behavior of the mixture [12]. The capillary rheometer is a common means of analyzing the shear rate behavior of a paste. Here, the paste flows through a varying die geometry and extrusion can be performed at varying extrusion velocities. The extrusion pressure- time/ displacement profiles represent the flow behavior as shown in *Figure 3* in section 2.3.[6, 13]

During extrusion, the solid and liquid phase are forced by a driving force for solid deformation and liquid movement. The liquid phase mobility is higher than the solid phase under an extrusion force. The liquid tends to fill the pores and redistribute. The redistribution is controlled by the permeability of a paste and liquid viscosity. The permeability of solid phase is determined by the stress that is generated during the extrusion process [6, 13]. However, the driving force of solid deformation is impeded by the frictional force between the particles, at the die, and barrel wall [13]. The paste is subjected to a shear along the die, barrel wall, and a deformation at the die entry as shown in *Figure 1* [14]. The shear along the die land is a function of extrusion velocity. The deformation of the materials in the die entry is inhomogeneous [15].

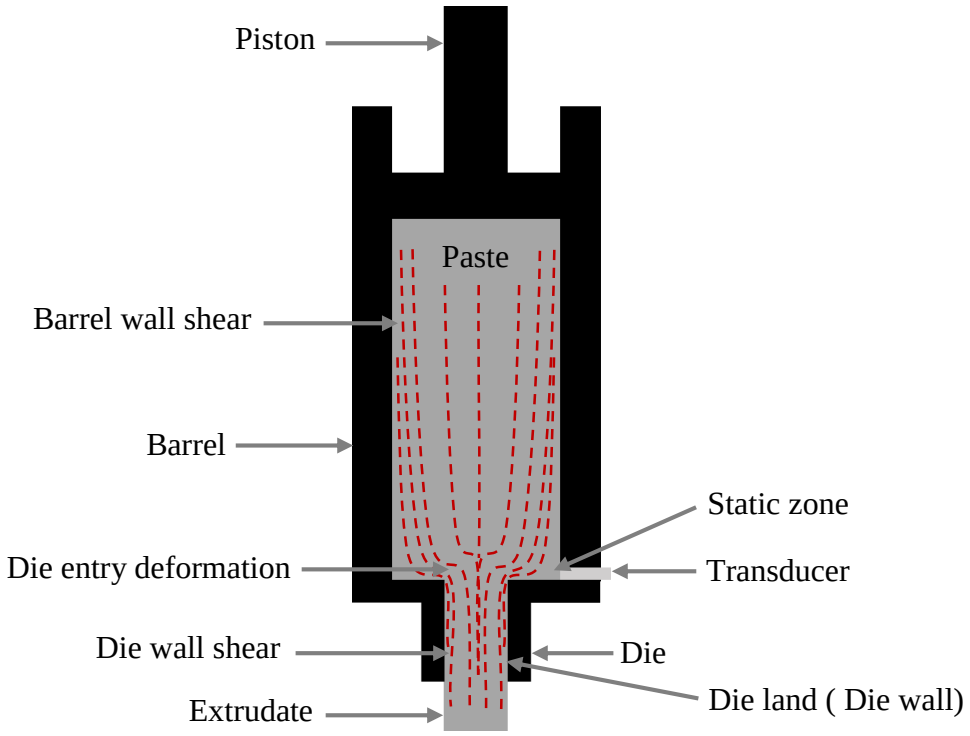

Figure 1: Shows a capillary rheometer with shear effect and die entry deformation.

1.2. Paste Formulation

The batch materials typically are water, binder, and micron or submicron particulates of powder all of them that form the paste. The batch materials could play an

important role in determining the green strength of extruded materials and the pore volume, pore distribution, and particle arrangement of extrudates.

Catalysts are produced using Titanium dioxide (TiO_2) have applications such as oil refining and energy production [5, 16]. Titanium dioxide (TiO_2) is used as a catalyst support because of its desirable properties such as high catalytic activity, and excellent thermal and chemical stability [7].

Previous studies have been done on the paste behavior and phase migration during the extrusion process without considering the microstructure and green strength. The water redistribution within the paste is related to initial water content, extrusion rate and die geometry [14]. Three materials (porcelain, earthenware, and terracotta) were studied in [17], the study showed that the ability of materials to be extruded is dependent on the plasticity of these materials that related to the initial composition and processing [17].

The challenges that are associated with the extrusion process are inhomogeneity, agglomeration, phase migration, and air bubbles. The water movement in the rheometer can cause pressure variations and surface defects as suggested in [18].

1.3. Extrusion Velocity

The extrusion pressure is a contribution of die entry pressure (die entry deformation) and die land pressure (wall shear) [5, 19]. One of these pressures can be dominated depending on the paste formulation such as the binder and water content [19]. In general, the pressure at a high extrusion velocity increases rapidly. The increase in pressure is because of high deformation at the die entry and/or high frictional shear along the die land [14, 18, 20]. Particles within the paste tend to pack effectively at a slower extrusion velocity and low shear stresses. Due to high shear stresses at the die wall, particle

packing is not effective [14, 18, 20]. There is a maximal liquid migration at a lower extrusion velocity as result of a high relative velocity of water within the paste; however, there is a liquid rheology dependence on liquid migration such as liquid viscosity [6, 13, 14, 18, 20]. A thin film of the liquid forms along the die land due to liquid migration at low extrusion velocities which provides a lubrication effect [6, 15, 19, 20]. This layer reduces the wall frictional shear at low velocity, but has no effect on the paste deformation at the die entry [15]. Although, the lubrication could cause extrusion failure as suggested in [19, 21].

The shear effect has been investigated in many studies without considering its effect on the microstructural, pore distribution, pore interconnectivity, and green strength. Non-uniform surface and macro defects in the extrudate can be linked to the extrusion velocity. Surface fracture happens at low and high velocities depending on the paste rheology [5, 18].

1.4. Image Quantitative Analysis and ImageJ

The conventional approach to investigating porosity in extruded materials is either mercury or helium porosimetry, but this technique does not provide a quantitative analysis of the pore spatial distribution. It can quite often lead to an underestimation of porosity because the fluid does not intrude the isolated pores [22, 23]. Image analysis techniques can be used to analyze a sequence of images and provide quantitative information on particle shape, porosity, and pore size distribution. The accuracy of the image analysis depends on image resolution, brightness/ contrast, and type segmentation approach followed [23]. There are several image analysis software available for 2 dimensional analysis ImageJ (National Institutes of Health, USA) being one of them. It is an open

platform Java based software and compatible with most of the image formats and operating systems. ImageJ has widely been used in a variety of applications to provide a quantitative analysis [23-26].

A number of segmentation approaches have been developed for image analysis [22, 23, 26, 27]. Such segmentation tool is thresholding. Thresholding an image is based on identifying individual pixels based on its intensity [28]. The pixel intensity is represented by a histogram. Phases, features, and points can be differentiated from each other based on the pixel intensity. The drawbacks of ImageJ thresholding are the lack of trustworthy, auto-assessment, and human interpretation [22, 26, 28].

1.5. Research Plan

1.5.1. Objective One: Optimal Formulation and Water Effect

The optimal formulation of TiO_2 paste was determined. The effect of varying the water content in the extruded TiO_2 will be shown to affect pore volume, densification, agglomeration size, and visible microdefects. A relationship between water content, mixing torque, extrusion pressure, green strength, and microstructural variability will be presented.

1.5.2. Objective Two: Extrusion Velocity Effect

The extrusion shear is influenced by many factors such as paste rheology and extrusion conditions. This section aims to understand the effect of extrusion velocity on the green strength as well as the microstructural variations in the sheared region (i.e. at the die wall) compared to an unsheared region. To quantify the porosity distribution, a number of images were extensively analyzed using a segmentation approach developed using ImageJ and Adobe Photoshop CC (Adobe Systems Inc., USA).

2. Experimental

2.1 Paste Formulation

2.1.1. Objective One: Optimal Paste Formulation and Water Effect

In this objective, G2 TiO_2 powder (Cristal Global, France) was mixed with sodium carboxymethyl cellulose (CMC) binder (Sigma-Aldrich, USA), and water to form a paste as shown in *Table 1*. To achieve an extrudable paste, the materials were pre-mixed in the dry state then pre-mixed by in a container with a spatula with water to form a wet mixture.

Table 1: Paste Formulations to study the effect of water content

CMC (%)	H_2O (%)
1.5	50.0-56.4
4.0	50.0-56.4

* (%) *based on G2 weight*

The wet mixture was mixed using a mixer to form a paste. The moisture content of pre-mixing and post-mixing materials was measured using a Computrac Moisture Analyzer (Arizona Instrument LLC, USA) to ensure that the water within the mixture and paste was constant.

2.1.2. Objective Two: Extrusion Velocity Effect

In Formulation A as shown in *Table 2*, G2 TiO_2 powder (Cristal Global, France) was pre-mixed with Hydroxypropyl Methylcellulose (HPMC) binder (The Dow Chemical Company, USA) in a dry state using Resodyn Acoustic mixer (Resodyn^{TM} Acoustic Mixers Inc., USA) at 100% intensity for 2.5 mins to obtain a well-mixed binder- powder distribution. Resodyn Acoustic mixer induces micro mixing zones. The mixer generates a mechanical resonance through the entire material [29]. Then, the blended powder is pre-mixed with H_2O by a container with a spatula to form a wet mixture.

In Formulation B as shown in *Table 2*, an aqueous of carboxymethyl cellulose (CMC) binder (Sigma-Aldric, USA) was used. A 1.5% CMC was mixed with a 56.4% H_2O using a magnetic stir for 10 min to form a high viscosity liquid. The resulting liquid has a higher viscosity than the water and this reduces the liquid migration during the extrusion process [20, 21]. The resulting liquid was pre-mixed with G2 TiO_2 powder with a spatula to form a wet mixture.

Table 2: Paste Formulations to study the effect of extrusion velocity

A	**B**
Dry mixture (TiO_2 and 2.4% HPMC binder) + 56.4% H2O	Liquid (56.4% H_2O with 1.5% CMC binder) + TiO_2

* (%) *based on G2 weight*

Then, the wet mixture was also loaded into a mixer to form a paste. The pastes were aged and sealed in a container at room temperature for 2 hr. to allow for the water equilibration within the paste [14]. The moisture content of pre-mixing, post-mixing, and post-aging materials were monitored using a Computrac Moisture Analyzer.

2.2 Torque Rheometer

The mixing behavior was monitored by a Haake Rheocord 9000 Torque Rheometer (Haake Buchler, USA). The mixer consists of a pair of sigma blades, a chute that provides the ability to load the wet mixture, and a water cooling system. Sigma blades shear and dispersive the materials between the blades and the wall of the chamber to form an extrudable paste. The water cooling system was used to mitigate the frictional heat challenge since the low temperature of mixing is important to get a homogenous and well binder- powder dispersion [30]. The temperature was monitored to keep it within a certain range (30.0-40.0) °C. The mixing time and speed were held constant at 100.0 RPM for 35.0 min to reach a degree of an acceptable mixedness.

Figure 2 shows the typical mixing behavior using a torque rheometer showing the loading peak torque as well as steady state mixing torque. The torque of mixing is the resistance of the mixture to the shear of the rotating blades. The lower torque value indicates a deagglomerated paste [30, 31].

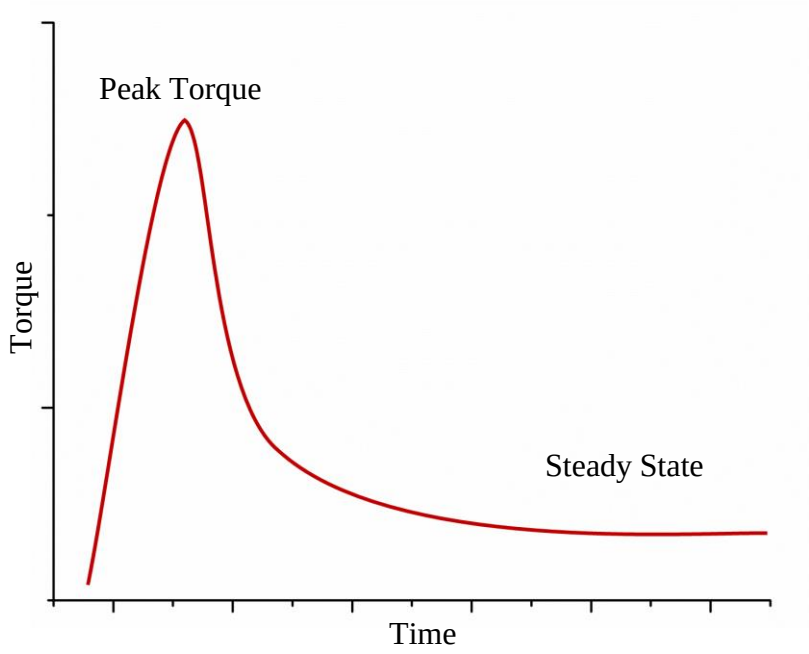

Figure 2: A typical mixing profile shows the mixing regions.

2.3 Capillary Rheometer

The extrusion experiments were conducted on the pastes at a constant velocity of 5 mm/min for extrusion experiment of objective one. The experiments were conducted at varying piston velocities (shear rate) (5.0, 10.0, 20.0, 30.0) mm/min for extrusion experiment of objective two. In this work, an RH2000 Capillary Rheometer (Malvern Instruments Ltd., UK) was used to study the rheology of the pastes. They were extruded through a cylindrical die with an 8.0 mm length, a 2.0 mm diameter, and an 180.0° die entry.

The precision of repeated measurements is 0.5% accurate for pressure transducers, less than 0.1% for piston velocity, 0.1% for temperature, and 5.0 microns for die precision. So, there is less than 5.0% off from repeated measurement (Malvern Instruments Ltd., UK).

The barrel was filled with the paste. The paste was tamped using a rod to remove the trapped air and compact the paste in the barrel. The ram was slowly lowered until it comes in contact directly with the top surface of the paste in the barrel pre-performing the test.

Figure 3 shows a typical extrusion profile for all pastes. At the outset of the extrusion, the pressure increases rapidly as the paste is compacted in the barrel under an extrusion velocity and pushed along the die wall. The pressure decreases at a point where the barrel wall shear is at a minimum. This point is measured as the extrusion pressure. Extrusion pressure then increases rapidly due to a high shear and extensive phases movement [5]. In some cases, there are fluctuations in the steady state pressure because of the phase migration, water redistribution, and trapped air [13]. The extrudates were collected prior to the rapid increase in pressure to minimize the influence of other high shear based factors on the microstructure. The extruded materials were placed in Thermolyne mechanical oven for about 24.0 hrs at 100.0 °C to ensure that the moisture was removed and the binder was not degraded.

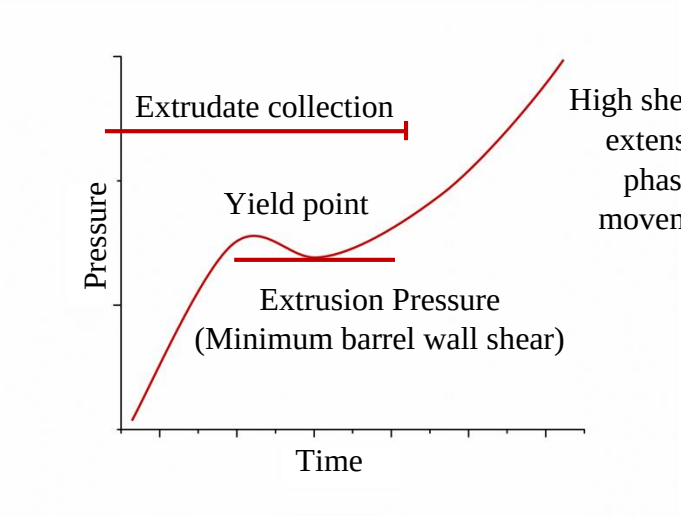

Figure 3: A typical extrusion profile.

2.4 Green Strength Measurement

The green strength of dried samples was measured using Kinexus Rotational Rheometer (Malvern Instruments Ltd, USA). The green strength measurement approach was developed in agreement with ASTM D6175-03 as described in [32]. Six cylindrical samples with approximately 2.0 mm diameter were selected randomly. The samples were sectioned into length between (2.0-4.0) mm to keep the length to diameter ratio equal or greater than 1:1 ratio [32]. The dried samples were placed between two flat surfaces, the top geometry (PU25) moves toward a stationary geometry (PL25) as shown in *Figure 4*.

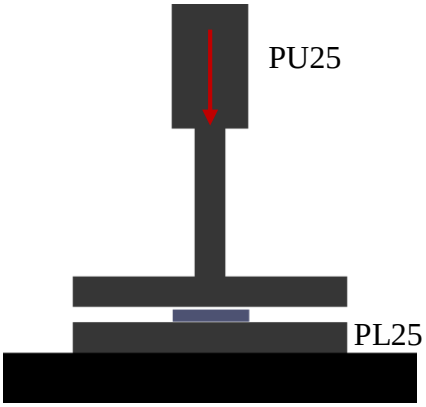

Figure 4: Schematic shows the top geometry (PU25) and the stationary geometry (PL25) of Kinexus Rotational Rheometer.

The green strength is described as force per extrudate length (F/L) as a function of the change in the extrudate diameter as shown in *Figure 5*.

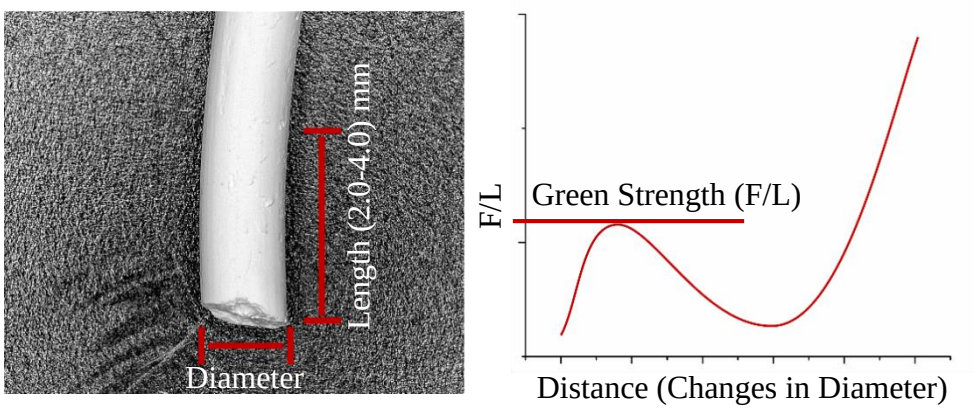

Figure 5: Extrudate image was acquitted using Keyence optical microscope (Keyence, USA) at 20.0x mag (left) and A typical green strength measurement profile (right).

2.5 Thermogravimetric Analysis

For further experiments, the binder must be removed. TGA (Thermogravimetric analysis) was conducted using the SDT Q600 (TA Instruments, USA) to determine the temperature of degradation that should be reached prior to the onset of sintering which typically begins above 750.0°C. The condition of the experiment was 10.0°C/min to 1400.0°C. The result indicates that the temperature of degradation is 650.0°C where the residual is about 23.0 wt% for CMC and about 4.0 wt.% for HPMC as shown in *Figure 6*. For subsequent handling, all extrudates were heat treated to 650.0°C in air.

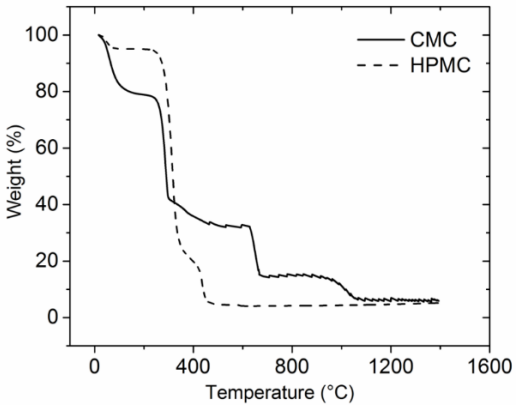

Figure 6: A degradation behavior of the binders.

2.6 Epoxy Infiltration Technique, Polishing, and Ion Milling

In binder free and dry extrudates, the porous microstructure was evaluated. This is challenging as the extrudate is weak. A metallurgical epoxy was used to fill the pores and allow for polishing and examination. This epoxy in addition to providing strength to the extrudate providing contrast with the titania and other phases for scanning electron microscope (SEM) analysis. Spurr's Kit (Electron Microscopy Science, USA) was used to embed the samples following the mix formula: 23.0% of ERL 4221, 18.0% of diglycidyl ether of polypropylene glycol (DER 736), 58.0% of nonenyl succinic anhydride (NSA), and 0.693% of dimethylaminoethanol (DMAE). The viscosity of epoxy was lowered at 60.0 °C for 15.0 min. The samples were kept under vacuum for 45.0 min to remove the bubbles that are formed within the epoxy. The infiltrated samples were cured at 70.0°C for 10.0 hrs. Infiltrated extrudates were mechanically polished using abrasive papers of 350, 600 and 1200 grits and (1.0, 0.25 and 0.05) µm diamond suspensions [24].

Ion milling technique was conducted for (3.5 – 4.0) hrs using a Hitachi IM 4000 ion mill (Hitachi, Japan). This step was applied to study objective two in this thesis. Surface imperfections such as pullouts and scratches can pose inaccuracies with image analysis. They increase human error and user bias. The quality of surface can improve image analysis and provide more reliable data. We have found that the mechanical polishing technique provides inaccuracies with image analysis; however, ion mill approach provides a high quality surface improving our image analysis.

The samples were fixed to the SEM stubs with carbon tape and coated with 15.0 nm of the gold layer to mitigate the charging issues.

2.7 Image Acquisition and Analysis

Images were acquitted using a Field Emission Scan Election Microscope (FESEM) (Zeiss, USA). The backscatter electron detector was used to provide a high contrast between different phases in the sample. Images were an indexed color mode with 1024 x 768 pixels and 8-bit channel. Images were obtained sequentially for each extrudate from the die wall (sheared region) to the center of the cross section with a 0.03 mm step using an FESEM stage navigator as shown in *Figure 7*. For the sake of simplicity, we assumed that the pore distribution is axisymmetric because of an axisymmetric die geometry was used.

Imaging was conducted at the same magnification, brightness, and contrast. A higher magnification FESEM (10.0K) was used to provide a high confidence in which the smaller pores included in the image with a reasonable number of images.

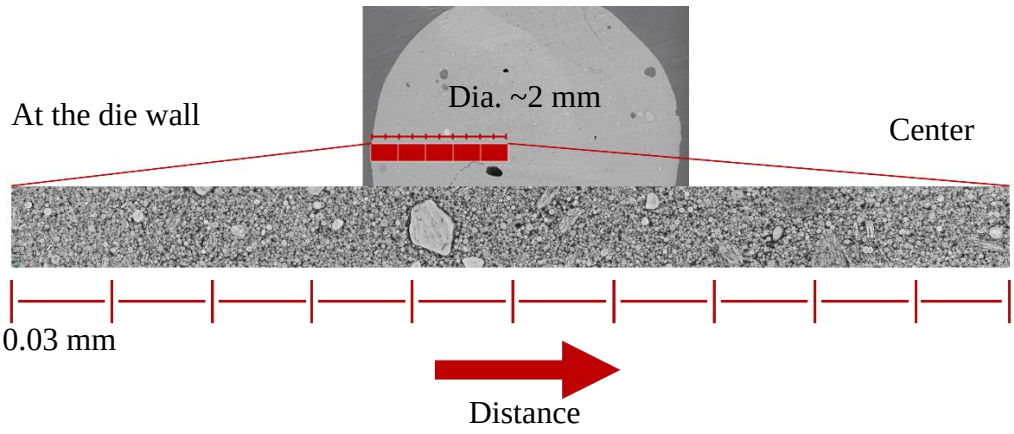

Figure 7: Extrudate cross section shows scanning direction and imaging step.

The intensity of pixels is between the low intensity dark pixel and high intensity bright pixel. The intensity values are between 0 (completely black) and 255 (completely white). Each pixel holds information that describes the image content. The intensity is affected by the brightness and contrast of the image [28]. The brightness and contrast were

adjusted using Adobe Photoshop CC to improve the user's acuity, segmentation accuracy, lower the uncertainty, and reduce the over-segmentation [23, 33]. The brightness and contrast adjustment was kept the same between the images.

The pore, crack, and epoxy pixel were assigned a single color. So, images can be parted into solid class (TiO_2) and pore/crack/ epoxy class. The darker pixels (low intensity) belong to the pore/ crack/ epoxy class and it distinctly different from the brighter pixels (high intensity) that belong to the solid class. "Intermediates shades of gray represent the transition in brightness that occurs as the solid component terminates into pores" [23, 33]. Based on that, the assumption was that the pixel color of pore/ crack/ epoxy has a certain range of the gray scale as indicated in *Figure 8*. This was applied for all images to keep the consistency and lower the user bias.

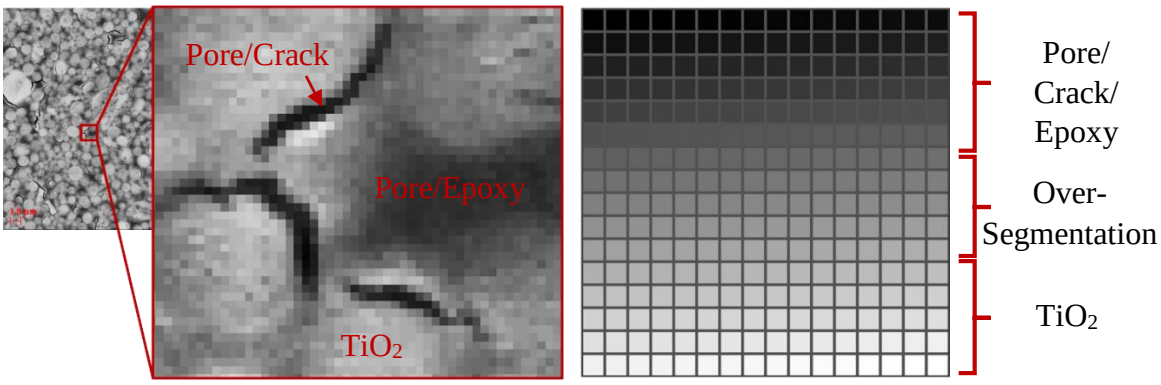

Figure 8: Shows typical phases of extrudate with distinguishable pixels (left) and the gray scale of the images as shown in Adobe Photoshop CC (right) where the pore/crack/ epoxy phase are black and near black pixels and TiO_2 phase is the brighter pixels.

The steps of segmentation are described:

1. Crop image to remove the information bar of the FESEM image. The image pixel will be 1024 x 692. This can be recorded and automated using Adobe Photoshop CC action.

2. The image must be converted to the grayscale mode in Adobe Photoshop (Image > mode> grayscale with 256 intensities as shown in *Figure 9*. This can be automated as well.
3. The brightness and contrast of gray level images can be adjusted in Adobe Photoshop CC (Image> Adjustments> Brightness/ Contrast). It must be kept the same among all the images. This step also can be automated in Adobe Photoshop CC.
4. The images must convert back to the indexed color mode with a gray level in Adobe Photoshop CC (Image>mode> Indexed Color). The indexed color images allow having a table of all the colors that is seen in an image. This step can be recorded using Adobe Photoshop CC action to automate it.
5. As we assumed above and shown in *Figure 8* that the pore/ crack/ epoxy pixel color range is black to near black color. Using Adobe Photoshop (Image> Mode> Color Table) allows changing the color of these pixels without affecting other pixels. In this work, the pixels were colored with a blue color (#0000ff). The idea is coloring certain pixels with a distinguishable color and to show that on the intensity of ImageJ histogram as shown in *Figure 9*. This can be automated using Adobe Photoshop. This must be applied to all images. The only factor that will play a role here is the amount of pore, crack, and epoxy are seen in an image. This minimizes user bias.
6. To determine the porosity in ImageJ (Image> Adjust> Threshold), the colored pixel then can be easily distinguished and thresholded. It based on the colored

intensity as shown in *Figure 9*. The percentage of the pixel can be input and used for other purposes.

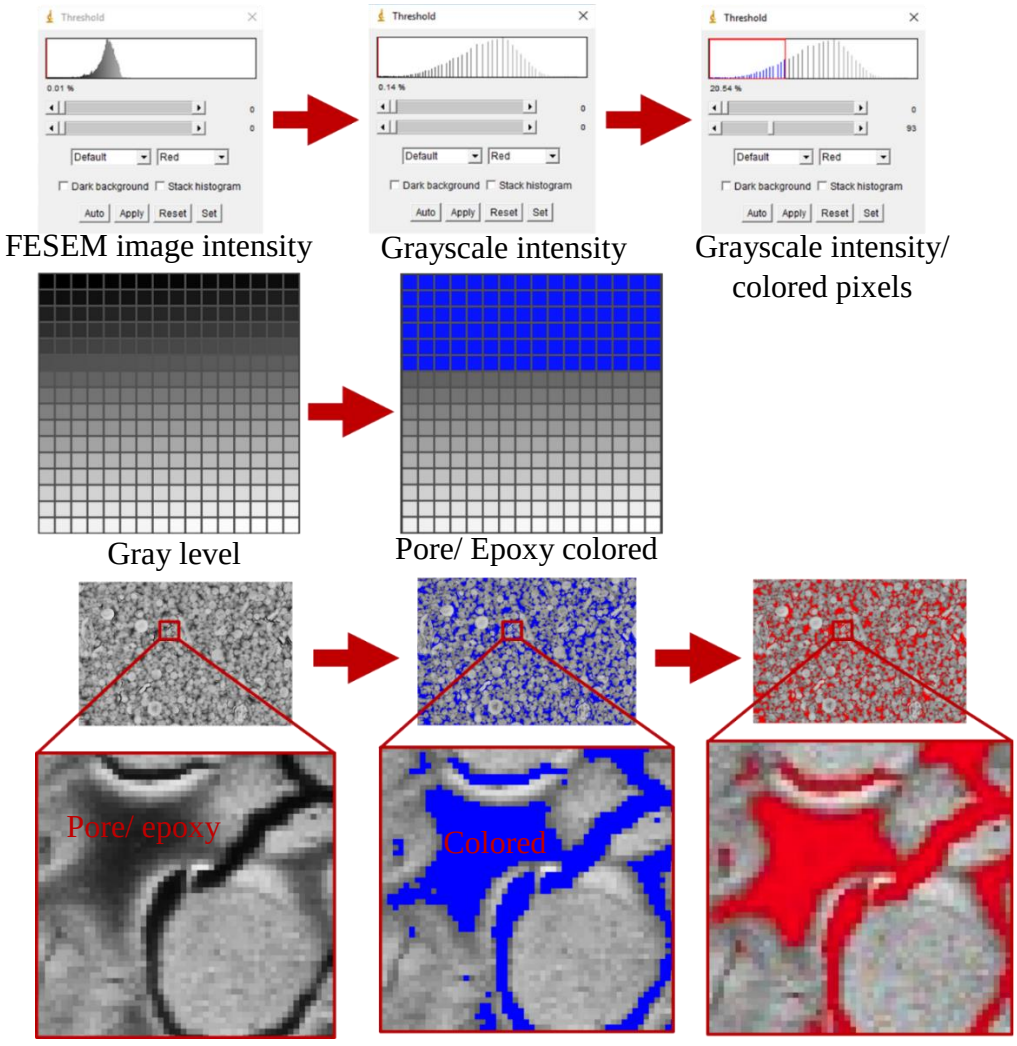

Figure 9: Shows segmentation details.

3. Results and Discussion

3.1. Objective One: Optimal Formulation and Water Effect

The results represent the mixing torque, extrusion pressure, green strength, and microstructure as a function of variation in water content. In this research objective, we will consider the high water (56.4%) and the low water (50.0%) content.

3.1.1. Torque Rheometer Analysis

Figure 10 below shows the peak torque of the high binder mixture is higher than the peak torque of the low binder mixture as it was expected. The high water content shows a lower peak torque. The low water mixture shows a higher steady state torque and a longer time to achieve steady state. On the contrary, the high water mixture shows a lower steady state torque and a shorter time to achieve steady state.

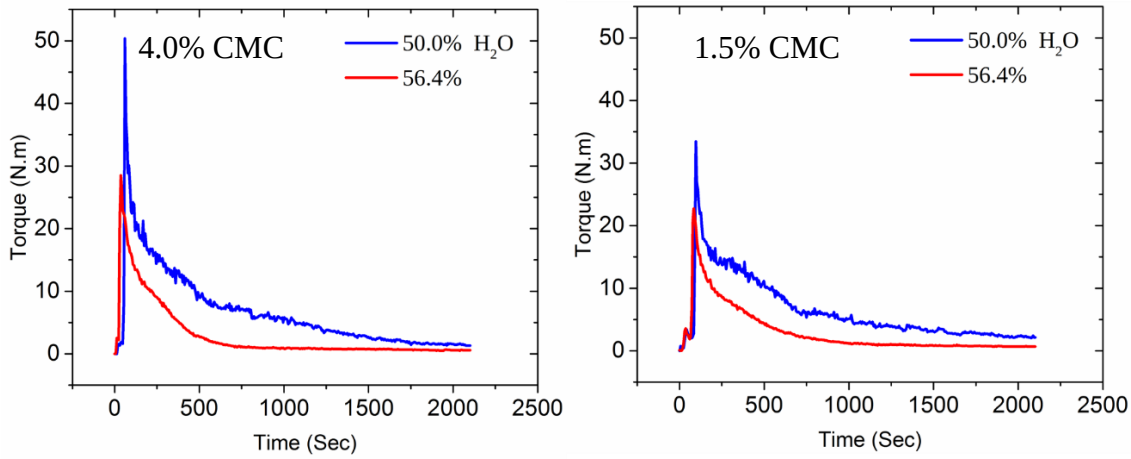

Figure 10: Mixing torque profile of varying water content for 1.5% and 4.0% CMC binder content.

A water range between high (56.4%) and low (50.0%) for the high and low binder mixture was investigated to study the steady state torque as shown in Figure 8. As the water content increases, the steady state torque decreases as shown in *Figure 11*.

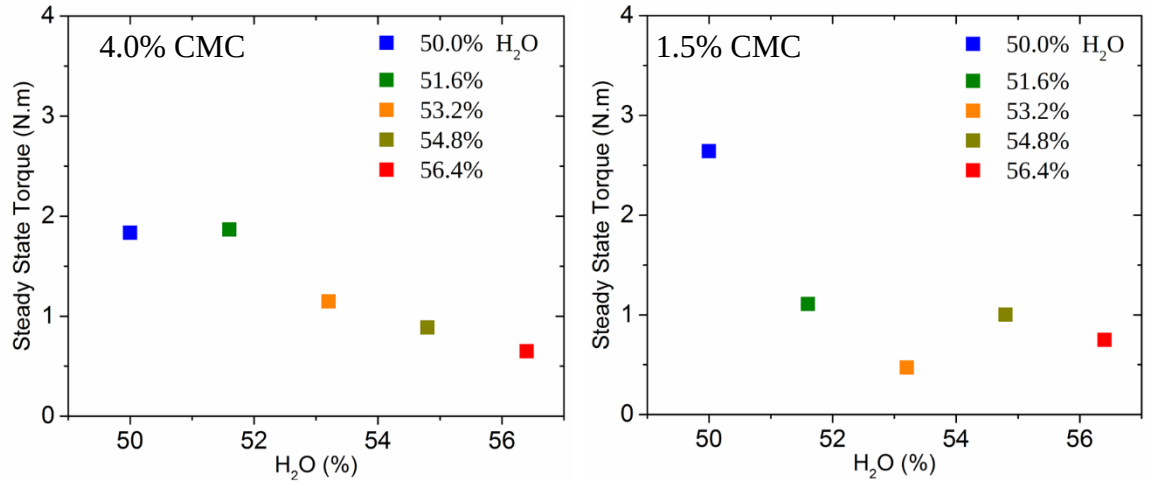

Figure 11: Steady state torque as a function of water content for 1.5% and 4.0% CMC binder content.

3.1.2. Capillary Rheometer Analysis

Figure 12 shows the capillary rheometer results for the different pastes examined. The results show that the extrusion pressure of high water paste is higher than the extrusion pressure of low water paste with both low and high binder. The increase in pressure might be due to a high die entry deformation. The steady state pressure duration is longer in the high water paste. The steady state extrusion pressure of the high water paste shows fluctuations because of phase movement and air bubbles.

The quality of the high water extrudate for high binder content was improved because there is enough water to form a thin layer of lubrication which lowered the effect of the extrusion shear along the die land.

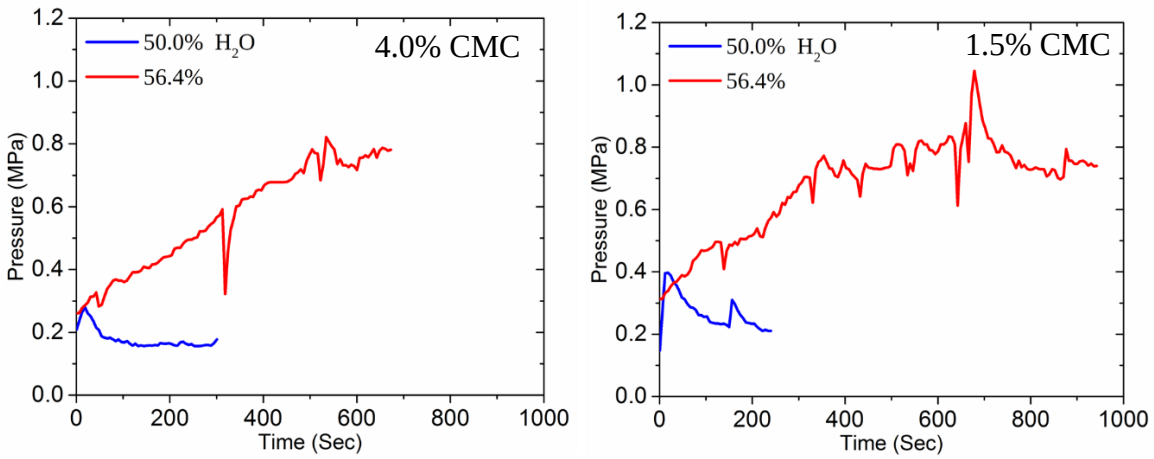

Figure 12: Extrusion profile of varying water content for 1.5% and 4.0% CMC binder content.

3.1.3. Green Strength Measurement

Figure 13 below shows that the green strength of high water extrudate is higher than the strength of low water extrudate. Previously as shown in *Figure 12* that the extrusion pressure of the high water paste is higher and vice versa. The high binder extrudate has lower green strength comparing to low binder extrudate.

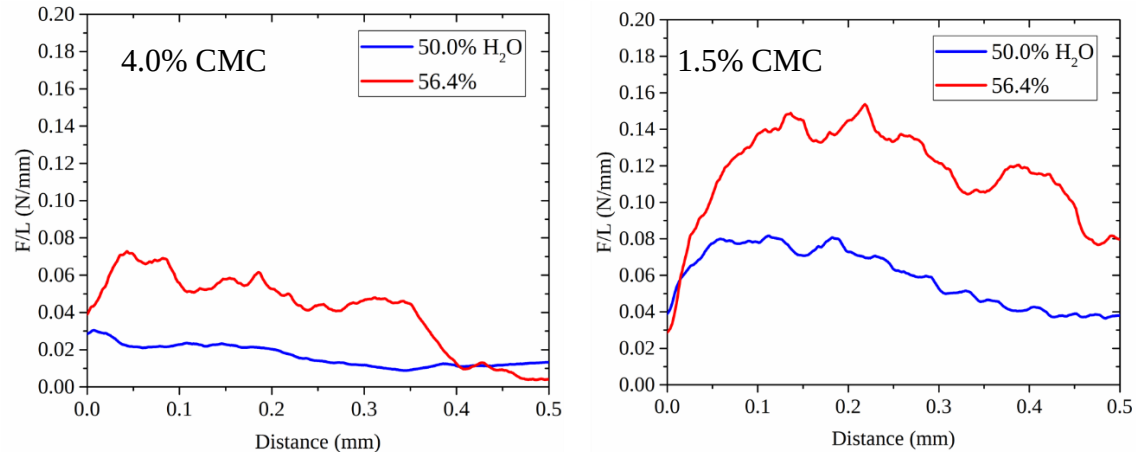

Figure 13: Shows the green strength of the low H_2O vs high H_2O for the low and high binder content.

3.1.4. Microstructural Variations

Figure 14 and Figure 15 show cross sections of low and high water extrudates. There are noticeable differences in the microstructure due to the water variations. The low

water extrudates have cracks and uneven pores size comparing to the high water extrudate. These defects can impact the green strength of the extrudates as shown in *Figure 13*.

In *Figure 14 and Figure* 15, the high water extrudate with low or high binder content are densified when compared to the low water extrudate with low or high binder content. The agglomerations size is larger in the case of the low water extrudate with low and high binder content.

56.4% H_2O 50.0% H_2O

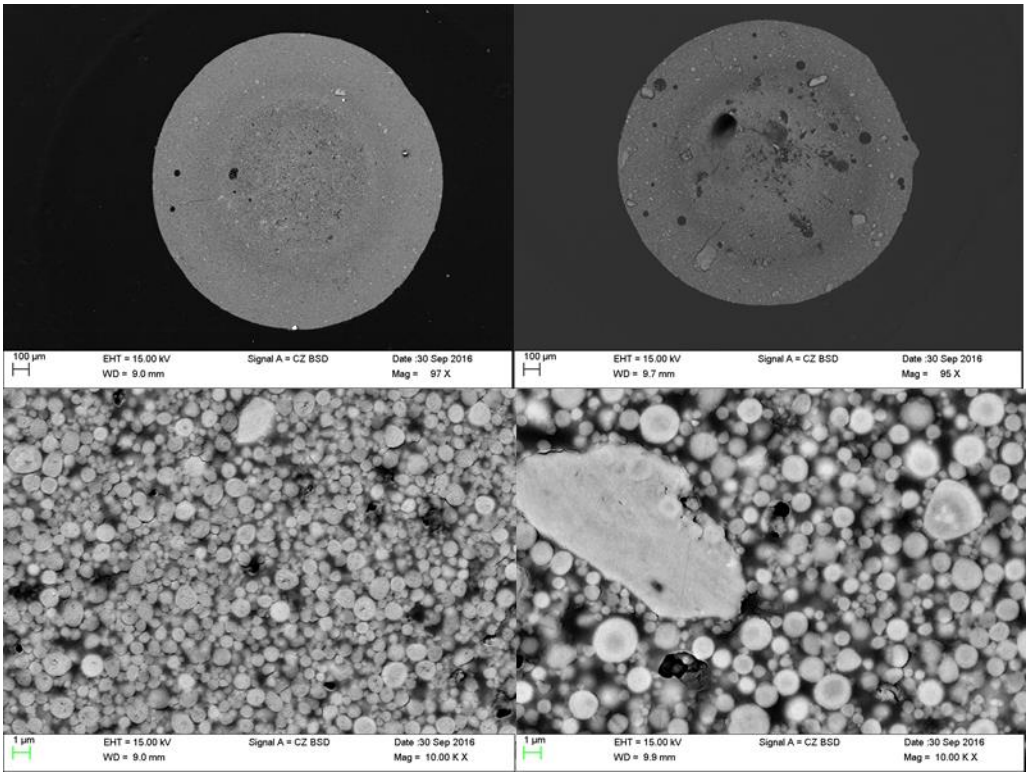

Figure 14: FESEM images of the extrudate cross section of low water content (left) vs high water content (right) for low binder content (1.5% CMC).

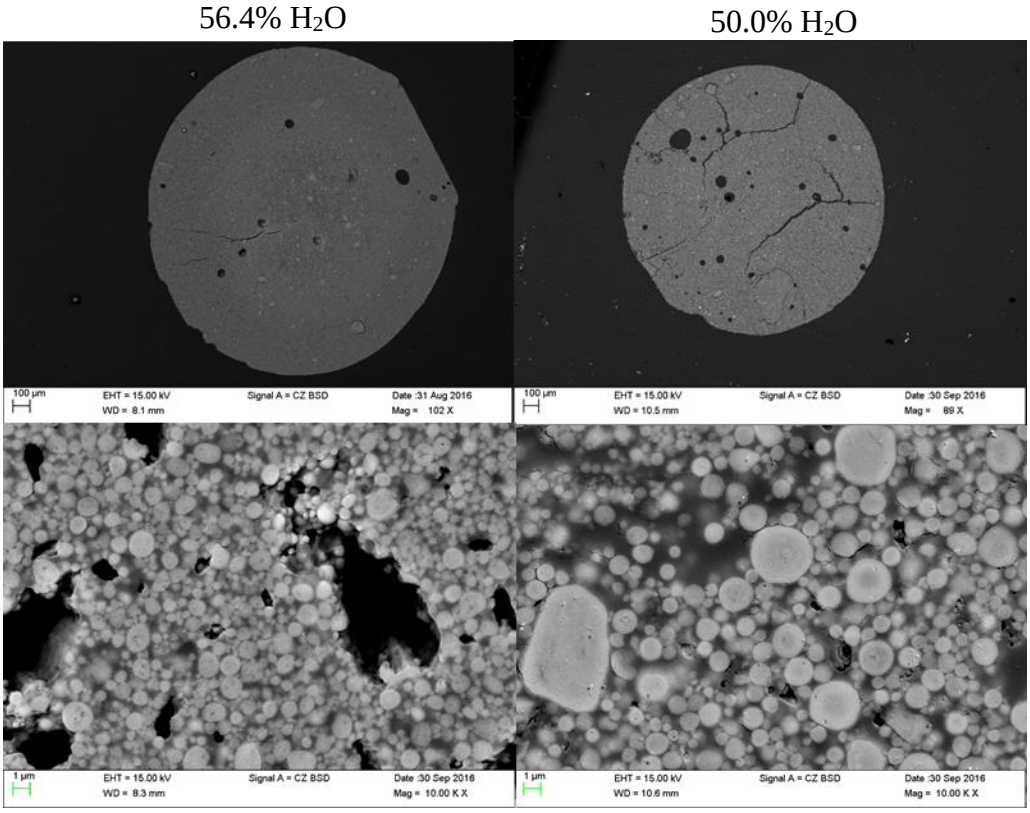

Figure 15: FESEM images of the extrudate cross section of low water content (left) vs high water content (right) for high binder content (4.0% CMC).

3.2 Objective Two: Extrusion Velocity Effect

The following results represent the extrusion velocity effect on both green strength and spatial variation of porosity. Although the aim is not to compare two different pastes, our observations on paste quality and extrudability will be mentioned briefly in this section.

3.2.1. Capillary rheometer Analysis

Figure 16 shows the extrusion pressure as a function of extrusion velocity. In the extrusion experiment with paste A, the extrusion increases at high extrusion velocity, although the increase is not as much as in B. The extrusion pressure is a combination of die entry deformation and frictional die wall shear. In some cases, one of them would dominate. Surface imperfection at a high velocity was observed as a consequence of frictional die wall shear. The layer of lubricating liquid was absent at high velocity due to

a limited liquid migration. These results suggest that the frictional die wall shear is higher comparing to die entry deformation.

In the extrusion experiment with paste B, the extrusion pressure increases as the extrusion velocity increases. The increase might be because of a high die entry deformation compared to the frictional die wall shear. A wet extrudate surface and drops of water at the die exit were observed. Hence, paste B shows a liquid migration effect compared to paste A. The layer of lubrication helps to mitigate the frictional die wall shear. The water movements at the die entry can increase the pressure as shown in section 3.1.2. It is interesting here to mention that the paste B is not as extrudable as paste A.

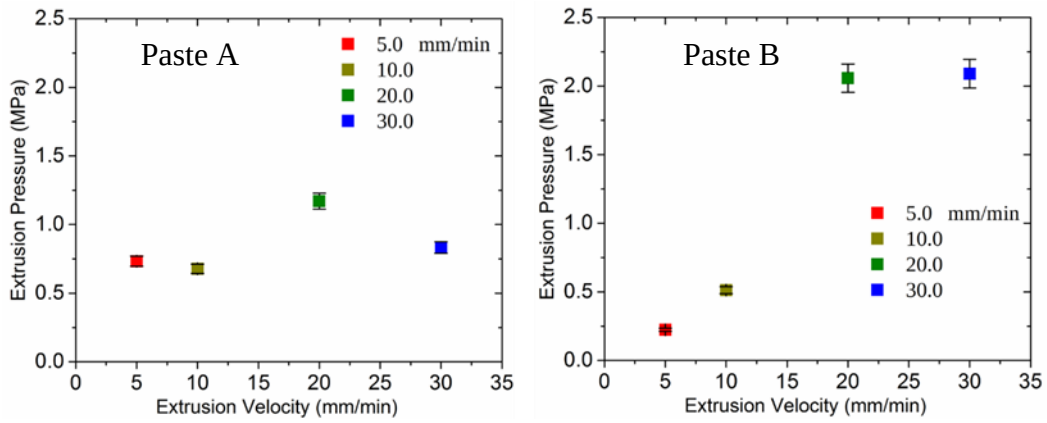

Figure 16: Extrusion pressure of paste A and paste B as a function of extrusion velocity, the error bars are 5% delta based on the precision of repeated measurement as discussed in section 2.3.

3.2.2. Green Strength Measurement

Figure 17 shows that the green strength of extrudate decreases as the extrusion velocity increases. The particles (powder and binder) do not densify effectively at a higher velocity as much as at the lower velocity. The low green strength might trace back to the frictional wall shear and die entry deformation.

It is interesting to note that the handling strength of extrudate of paste A was higher compared to the extrudate of paste B. This observation is reflected in the green strength data of dried extrudate as shown in *Figure 17*.

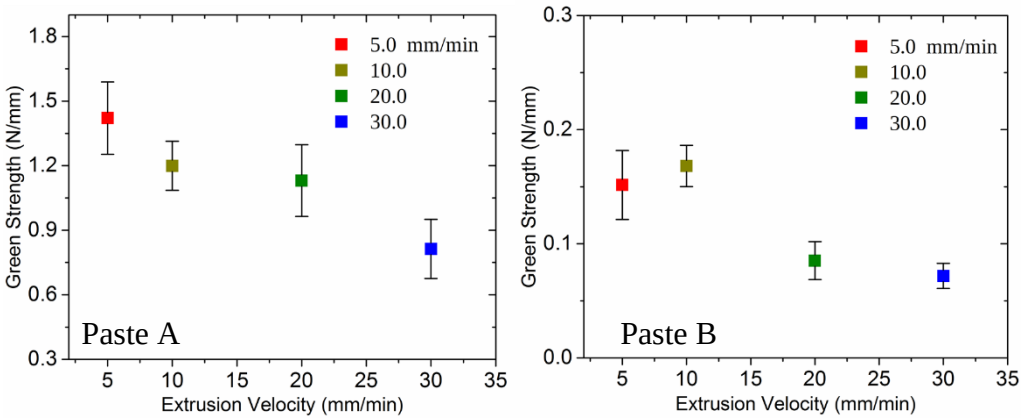

Figure 17: Green Strength of an extrudate of paste A and paste B as a function of velocity, the error bars represent the standard deviation error for n= six samples/batch.

3.2.3. Microstructural Spatial Variations

Figure 18 shows a histogram of porosity distribution from at the die wall toward the center of the extrudate cross section for both paste A and B.

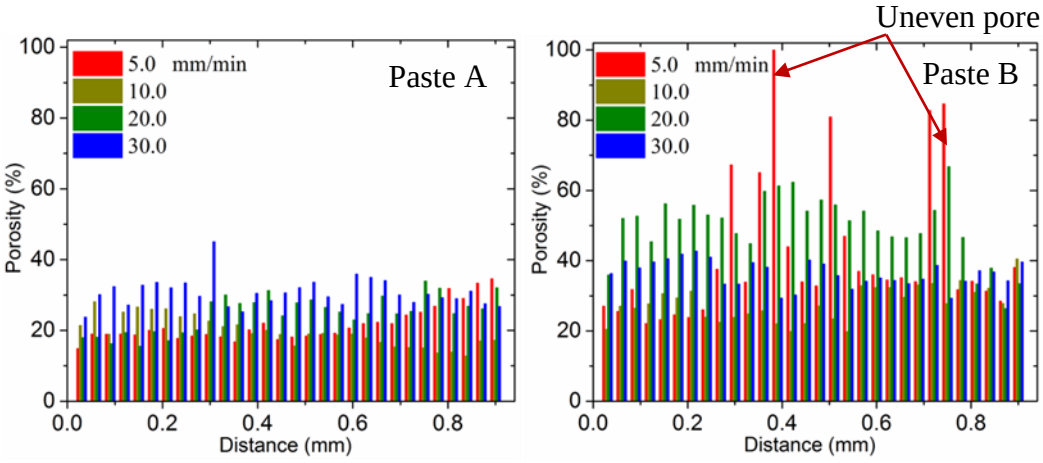

Figure 18: Spatial variations of porosity at the die wall (distance is around 0 mm) toward the center of extrudate cross section (distance is around 0.9 mm).

Paste A: In *Figure 19*, samples that were extruded at a velocity of 5 mm/min shows a lower porosity at the die wall when compared to the center region of extrudate cross section (unsheared region). On the contrary, samples that were extruded at a velocity of 10

mm/min show a high porosity at the die wall compared to the center region of extrudate cross section (unsheared region).

There is no trend in the spatial variations of porosity for samples that were extruded at velocities of (20 and 30) mm/min, although at the die wall shows a high porosity comparing to samples that were extruded at a velocity of 5 mm/min.

Paste B: In *Figure 20*, samples that were extruded at velocities of (5 and 10) mm/min show a lower porosity at the die wall, but there is no trend compared to the center of the extrudate cross section (unsheared region). Conversely, for samples that were extruded at velocities of (20 and 30) mm/min shows a high porosity at the die wall compared to the center of extrudate cross section (unsheared region).

Samples that were extruded at high velocity show a high porosity at the die wall compared to the low velocity extrudate. The FESEM images show that the high velocity extrudate is not as densified as the low velocity extrudate. The samples that were extruded with paste B show uneven pores as shown in the histogram of pore distribution in *Figure* 18.

The spatial variations of porosity can be affected by varying factors such as liquid migration, frictional die wall shear, and die entry deformation.

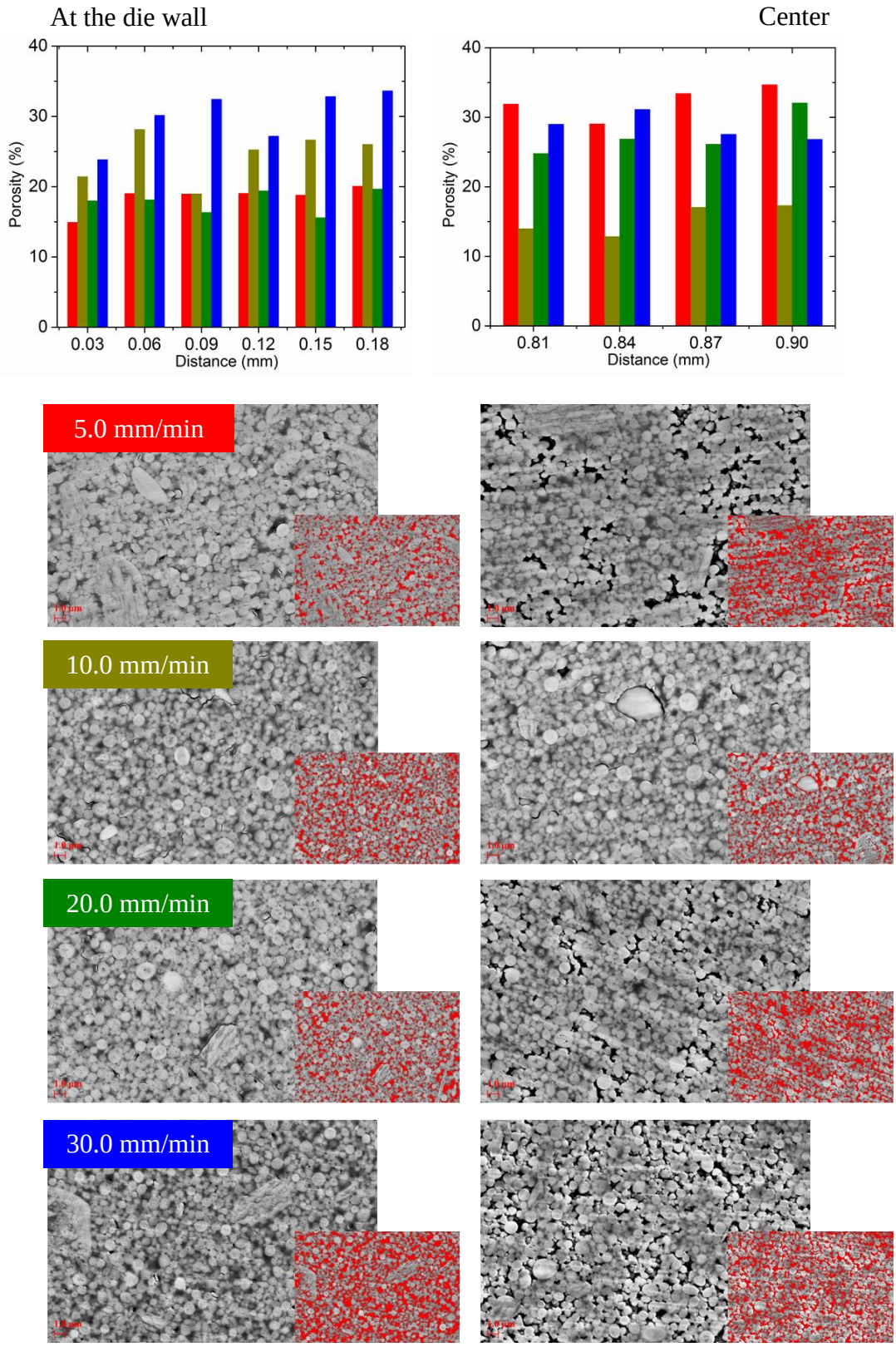

Figure 19: Shows a histogram of pore distribution from at the die wall (left) to the center (right) of the cross section for paste A. Typical images of at die wall and the center region for various velocities.

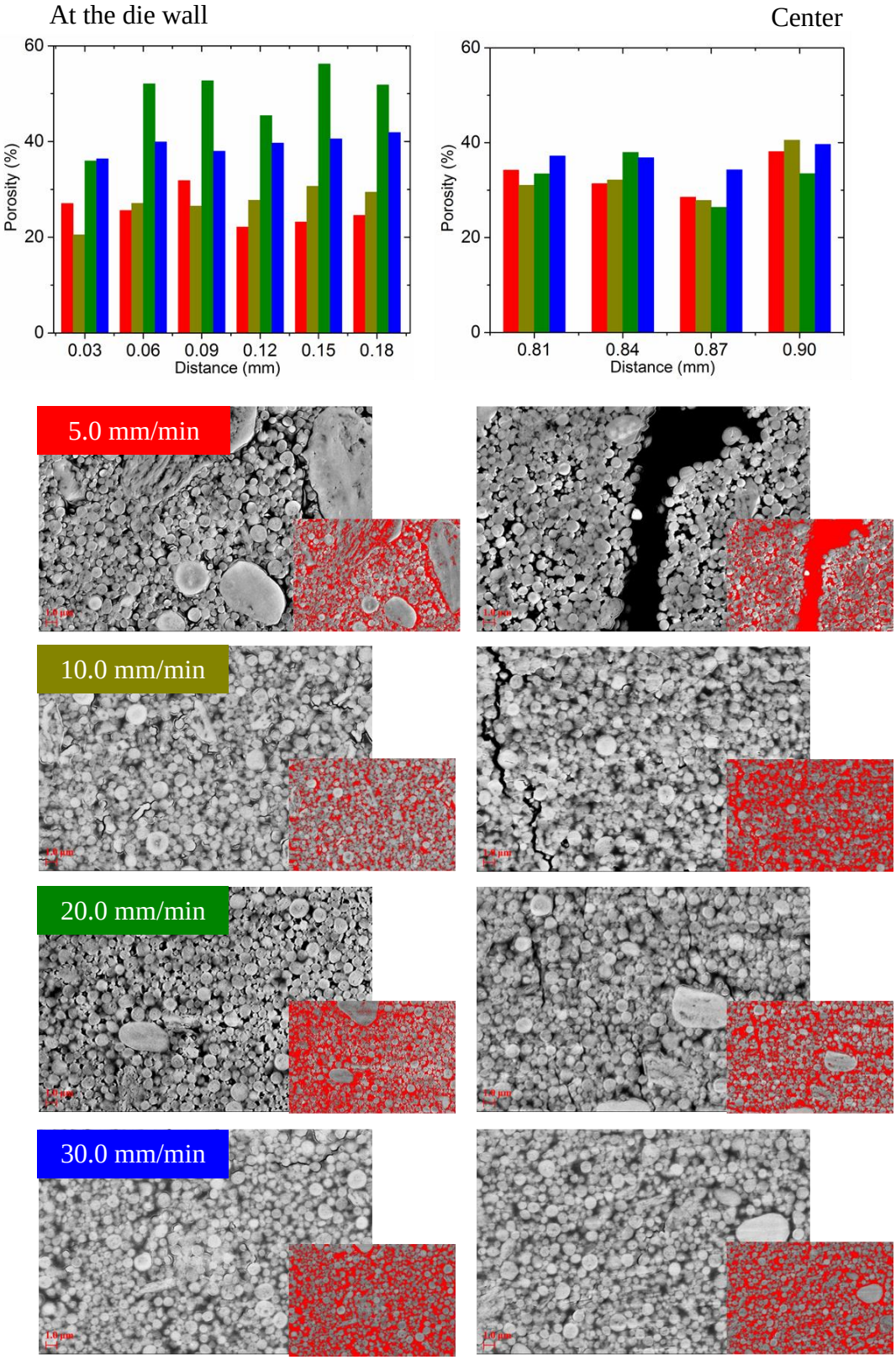

Figure 20: Shows a histogram of pore distribution from at the die wall (left) to the center (right) of the cross section for paste B. Typical images of at die wall and the center region for various velocities.

4. Conclusions

4.1. Objective One: Optimal Formulation and Water Effect

There is a relationship between torque rheometer and capillary rheometer analyses, green strength, and microstructural variability for titania pastes and extrudates varying water content were showed. The high water content pastes/ extrudates with low or high binder content show a lower mixing torque and a shorter time to achieve the steady state. The extrusion pressure increases as the water content increases. The high water content can result in improved green strength of extrudate. The water content factor can be caused a microstructural variability. The microdefects are lowered using a high water content. There are variations in densification due to varying water content, with lower water content pastes/ extrudates commonly being more porous.

4.2. Objective Two: Extrusion Velocity Effect

The relationship between the extrusion velocity, green strength, and spatial variations of porosity of extrudate is presented. The extrusion pressure is a combination of die entry deformation and frictional die wall shear. One of these would dominate depending on the paste formulation. In general, the extrusion pressure increases as the extrusion velocity increases. Surface imperfection was observed at a high extrusion velocity. A segmentation approach was developed to quantify the spatial variation of extrudate porosity. The extrusion velocity can cause a spatial variation of porosity. The low extrusion velocity shows a low porosity in the sheared region (at the die wall) compared to the unsheared region and vice versa. The green strength of extrudate can be improved at low extrusion velocity.

Finally, HPMC binder showed a high extrudability and strength compared to CMC binder. Therefore, we do not recommend to use CMC binder in extrusion application based on the results were showed in this work.

5. Future Work

1. Examine the effect of using an aqueous of varying binder contents and compositions on the green strength and microstructural variability of extrudate. The rheological properties of liquids, such as viscosity in this study [20], suggest that the properties of a paste are related to the liquid rheology.

2. Aged paste at different stages of paste equilibration should be used to study the paste flow, microstructural variability, and green strength of extrudate. What impact does aging time have on the spatial variation of porosity?

3. A chopped fiber, i.e. fiber glass can be added to the paste. Correlate the extrusion conditions, such as die geometry and extrusion velocity, and the fiber spatial distribution.

4. Perform torque rheometer using different blade geometries and mixing conditions. One suggestion would be to use a roller blade which results in a very high shear rate. It may lead to enhanced mixedness and reduce the size of agglomerates.

5. In a couple of studies [5, 18], a longer die land was found to reduce the surface fracture of extrudate. The shear friction of varying die geometries should be investigated on the green strength and spatial variation of porosity of the extrudate.

6. A quantitative method of 2-D visualization and segmentation for non-axisymmetric die geometry and second phase additive (chopped fiber) should be developed.

7. A quantitative method of 3-D visualization and segmentation could be developed. The resulting approach could be used to study the effect of paste formulation, mixing, and extrusion conditions on the microstructural variability, porosity distribution,

and pore interconnectivity, especially in the sheared region (at the die wall). Mercury porosimetry data must be compared with the 3-D image analysis data.

8. According to Benbow *et al.* [5], the initial bulk stress ($\sigma_\circ$), initial wall shear ($\tau_\circ$), and velocity dependence parameters of the flow into the die and along the die land can be determined using at least two varying die lengths and extrusion velocities [5]. These parameters may depend on paste rheology, mixing, and extrusion conditions. These parameters can be correlated to the spatial variations of porosity and green strength of extrudate.

6. Reference

[1] R. Matyssek, N. Clarke, P. Cudlín, T. N. Mikkelsen, J.-P. Tuovinen, G. Wieser, *et al.*, *Climate change, air pollution and global challenges: understanding and perspectives from forest research* vol. 13: Newnes, 2013.

[2] T. R. Karl and K. E. Trenberth, "Modern global climate change," *science,* vol. 302, pp. 1719-1723, 2003.

[3] T. C. S. o. Japan and N. S. Kyōkai, *Advanced Ceramic Technologies & Products*: Springer Science & Business Media, 2012.

[4] R. M. Heck, R. J. Farrauto, and S. T. Gulati, *Catalytic air pollution control: commercial technology*: John Wiley & Sons, 2009.

[5] J. Benbow and J. Bridgwater, "Paste flow and extrusion," 1993.

[6] A. Yu, J. Bridgwater, A. Burbidge, and Z. Saracevic, "Liquid maldistribution in particulate paste extrusion," *Powder Technology,* vol. 103, pp. 103-109, 1999.

[7] S. Bagheri, N. Muhd Julkapli, and S. Bee Abd Hamid, "Titanium dioxide as a catalyst support in heterogeneous catalysis," *The Scientific World Journal,* vol. 2014, 2014.

[8] J. A. Lapszewicz, H. J. Loeh, and J. R. Chipperfield, "The effect of catalyst porosity on methane selectivity in the Fischer–Tropsch reaction," *Journal of the Chemical Society, Chemical Communications,* pp. 913-914, 1993.

[9] M. A. Vannice and W. H. Joyce, *Kinetics of catalytic reactions* vol. 134: Springer, 2005.

[10] Y. Lee, T. Kim, and Y. Choi, "Effect of porosity in catalyst layers on direct methanol fuel cell performances," *Fuel Cells,* vol. 13, pp. 173-180, 2013.

[11] A. Fischer, J. Jindra, and H. Wendt, "Porosity and catalyst utilization of thin layer cathodes in air operated PEM-fuel cells," *Journal of Applied Electrochemistry,* vol. 28, pp. 277-282, 1998.

[12] B. Cheng, C. Zhou, W. Yu, and X. Sun, "Evaluation of rheological parameters of polymer melts in torque rheometers," *Polymer Testing,* vol. 20, pp. 811-818, 2001.

[13] S. Rough, D. Wilson, and J. Bridgwater, "A model describing liquid phase migration within an extruding microcrystalline cellulose paste," *Chemical Engineering Research and Design,* vol. 80, pp. 701-714, 2002.

[14] S. Rough, J. Bridgwater, and D. Wilson, "Effects of liquid phase migration on extrusion of microcrystalline cellulose pastes," *International journal of pharmaceutics,* vol. 204, pp. 117-126, 2000.

[15] D. Horrobin and R. Nedderman, "Die entry pressure drops in paste extrusion," *Chemical Engineering Science,* vol. 53, pp. 3215-3225, 1998.

[16] L. Chevalier, E. Hammond, and A. Poitou, "Extrusion of TiO 2 ceramic powder paste," *Journal of materials processing technology,* vol. 72, pp. 243-248, 1997.

[17] P. Guilherme, M. Ribeiro, and J. Labrincha, "Behaviour of different industrial ceramic pastes in extrusion process," *Advances in Applied Ceramics,* vol. 108, pp. 347-351, 2009.

[18] S. Majidi, G. H. Motlagh, B. Bahramian, B. Kaffashi, S. A. Nojoumi, and I. Haririan, "Rheological evaluation of wet masses for the preparation of pharmaceutical pellets by capillary and rotational rheometers," *Pharmaceutical development and technology,* vol. 18, pp. 112-120, 2013.

[19] R. N. Das, C. Madhusoodana, and K. Okada, "Rheological studies on cordierite honeycomb extrusion," *Journal of the European Ceramic Society,* vol. 22, pp. 2893-2900, 2002.
[20] J. Benbow, S. Blackburn, and H. Mills, "The effects of liquid-phase rheology on the extrusion behaviour of paste," *Journal of materials science,* vol. 33, pp. 5827-5833, 1998.
[21] Y. Chen, A. Burbidge, and J. Bridgwater, "Effect of carbohydrate on the rheological parameters of paste extrusion," *Journal of the American Ceramic Society,* vol. 80, pp. 1841-1850, 1997.
[22] S. Rajagopalan, L. Lu, M. J. Yaszemski, and R. A. Robb, "Optimal segmentation of microcomputed tomographic images of porous tissue-engineering scaffolds," *Journal of Biomedical Materials Research Part A,* vol. 75, pp. 877-887, 2005.
[23] V. Guarino, A. Guaccio, P. A. Netti, and L. Ambrosio, "Image processing and fractal box counting: user-assisted method for multi-scale porous scaffold characterization," *Journal of Materials Science: Materials in Medicine,* vol. 21, pp. 3109-3118, 2010.
[24] N. Ku, "Evaluation of the behavior of ceramic powders under mechanical vibration and its effect on the mechancis of auto-granulation," Doctor of Philosophy, Materials Science and Engineering, Rutgers. The State Univeristy of New Jersey, Graduate School- New Brunswick, 2015.
[25] E. C. Jensen, "Quantitative analysis of histological staining and fluorescence using ImageJ," *The Anatomical Record,* vol. 296, pp. 378-381, 2013.
[26] C. Grove and D. A. Jerram, "jPOR: An ImageJ macro to quantify total optical porosity from blue-stained thin sections," *Computers & Geosciences,* vol. 37, pp. 1850-1859, 2011.
[27] C.-T. Li, "Multiresolution image segmentation integrating Gibbs sampler and region merging algorithm," *Signal Processing,* vol. 83, pp. 67-78, 2003.
[28] J. M. M. Pérez and J. Pascau, *Image processing with ImageJ*: Packt Publishing Ltd, 2013.
[29] J. G. Osorio and F. J. Muzzio, "Evaluation of resonant acoustic mixing performance," *Powder Technology,* vol. 278, pp. 46-56, 2015.
[30] R. Supati, N. Loh, K. Khor, and S. Tor, "Mixing and characterization of feedstock for powder injection molding," *Materials Letters,* vol. 46, pp. 109-114, 2000.
[31] P. Suri, S. V. Atre, R. M. German, and J. P. de Souza, "Effect of mixing on the rheology and particle characteristics of tungsten-based powder injection molding feedstock," *Materials Science and Engineering: A,* vol. 356, pp. 337-344, 2003.
[32] "Standard Test Method for Radial Crush Strength of Extruded Catalyst and Catalyst Carrier Particles," ed: ASTM International, 2013.
[33] "Standard Guide for Interpreting Images of Polymeric Tissue Scaffolds," ed: ASTM International, 2012.